International Journal of Applied Science and Engineering
2009. 7, 1: 79-93

Damage Identification of a Thin Plate in the Time Domain with Substructuring-an Application of Inverse Problem

S.Sandesh[a] and K. Shankar[b*]

[a]*Research Scholar, Department of Mechanical Engineering, IIT Madras.*
[b]*(corresponding author) Assistant Professor, Department of Mechanical Engineering, IIT Madras, Chennai India 600036.*

Abstract: Damage in a plate in the form of a line crack contained in an element, and oriented at an arbitrary angle is detected using an inverse time domain formulation. The time domain acceleration responses need to be measured at certain locations. The crack damage is modeled using an equivalent orthotropic finite element scheme based on the strain energy equivalence principle. The principle is to minimize the difference between the measured and theoretically predicted accelerations. Since the computational effort of identification using the global finite element model of the plate proved prohibitive, the substructure method was used. The substructure was further condensed of the rotary DOF's for increased computational improvement. In order to identify the location and magnitude of the damage variables, acceleration responses at the substructure interfaces and also a few selected points inside the substructure are required. Using numerically simulated experiments the crack was reliably detected using this method. The damage is identified with the addition of noise as well as at different forcing frequencies. The Genetic Algorithm (GA) and Particle Swarm Optimization (PSO) were used to solve the inverse problem. The PSO algorithm proved superior to GA in convergence and accuracy.

Keywords: System Identification; Damage detection; Time domain; Substructure.

1. Introduction

Inverse problems often occur in many branches of engineering fields where the values of certain physical model parameters are required to be recovered from observed data. System identification (SI) comes under the category of inverse problem. It is a process of determining the parameters of a system based on the observed input and output (I/O) of the system. The application of SI technique presented here illustrates the damage detection of a uniform thin plate based on the vibration data. Doebling *et al.* has presented a comprehensive survey of vibration based damage detection methods [1]. The development of modal analysis techniques for damage detections arose from the observation that the structural properties affect the natural frequencies, mode shapes and frequency response function (FRF) etc. Many researchers have used one or several of these characteristics to detect and locate damages in the structures. Young Shin Lee and Chung used the first four natural frequencies of the cantilever beam to identify

* Corresponding author; e-mail: skris@iitm.ac.in
Accepted for Publication: April 08, 2009

a designated crack [2]. Wang *et al*. presented a damage detection scheme in which static deformations and natural frequencies of planar trusses and beams are applied with an interactive optimization algorithm to assess the location and severity of specific damages [3]. Hwang and Kim used subset of vectors from full set of FRFs for a few frequencies measurements to detect the location and severity of damages [4]. Araujo *et al.* proposed damage identification method based on FRF sensitivities [5]. The damage identification was performed on a laminated rectangular plate, discretized using a finite element (FE) model. Lee *et.al* has shown that damage in the form of a crack in an isotropic small material volume can be represented by an equivalent continuum model with orthotropic properties, producing the same strain at the boundaries [6]. This model was used in a study to predict crack damage in a plate using frequency response data [7]. Surface crack detection in composite laminates by modal analysis and strain energy method was carried out in [8]. Here the FE model of a composite laminate was obtained using ANSYS and the results were validated using experiments. In order to deal with the computational effort in identifying systems with many unknowns which result in large DOF (Degree-of-Freedom) models Koh *et al.,* proposed a substructure system identification scheme [9]. They also present a summary of various substructure approaches used in parametric system identification in the time-domain. An ideal substructure method is one which could identify all parameters in a given substructure without the need to estimate or know any parameters outside that substructure. Also, all the measurement sensors must be confined inside that specific substructure.

With recent rapid advances in computer hardware and improved computational methods, application of SI as an inverse problem for damage detection has grown rapidly. Random search intelligent algorithms such as Genetic Algorithms (GA) and Particle Swarm Optimization (PSO) have been applied in system identification [9, 10, 11] due to their robustness and ability to handle many damage variables.

This paper presents a new time-domain damage detection scheme based on substructure system identification method using GA or PSO to filter out the correct parameters from a given search domain. The algorithm estimates the damage parameters through minimization of an error function defined by mean squared error between the measured and estimated accelerations at all time steps and all locations. The measured values are obtained from an experiment; this is numerically simulated from a known model in this case. Estimated values are obtained from a known mathematical (i.e., finite element) model.

2. Time domain substructure method

Computational effort increases with the number of parameters to be identified. It therefore makes sense to divide the structure into smaller substructures, for which numerical convergence can be achieved more easily. The time domain substructure method followed here is derived from [12]. The equation of motion for the complete structural system is given by,

$$M\,\ddot{x}(t) + C\,\dot{x}(t) + K\,x(t) = P(t) \tag{1}$$

where M, C, K and $P(t)$ are the mass, damping stiffness matrices and excitation force vector, respectively. The Raleigh damping approach where $C = aM + bK$, where α and β are two coefficients decided by the user from modal information of two modes.

The partitioned equations for the structure shown in Figure1 are written as,

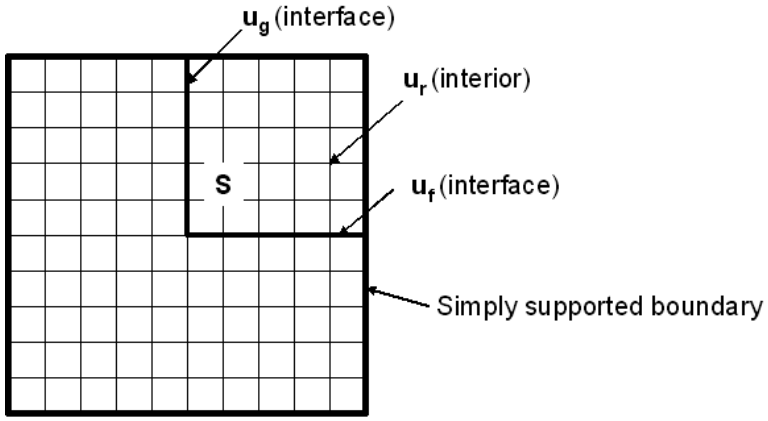

Figure 1. Global structure and substructure (S) of the plate

$$\begin{bmatrix} M_{uu} & M_{uf} & & & & \\ M_{fu} & M_{ff} & M_{fr} & & & \\ & M_{rf} & M_{rr} & M_{rg} & & \\ & & M_{gr} & M_{gg} & M_{gd} & \\ & & & M_{dg} & M_{dd} \end{bmatrix} \begin{Bmatrix} \ddot{x}_u \\ \ddot{x}_f \\ \ddot{x}_r \\ \ddot{x}_g \\ \ddot{x}_d \end{Bmatrix} + \begin{bmatrix} C_{uu} & C_{uf} & & & & \\ C_{fu} & C_{ff} & C_{fr} & & & \\ & C_{rf} & C_{rr} & C_{rg} & & \\ & & C_{gr} & C_{gg} & C_{gd} & \\ & & & C_{dg} & C_{dd} \end{bmatrix} \begin{Bmatrix} \dot{x}_u \\ \dot{x}_f \\ \dot{x}_r \\ \dot{x}_g \\ \dot{x}_d \end{Bmatrix}$$
$$+ \begin{bmatrix} K_{uu} & K_{uf} & & & & \\ K_{fu} & K_{ff} & K_{fr} & & & \\ & K_{rf} & K_{rr} & K_{rg} & & \\ & & K_{gr} & K_{gg} & K_{gd} & \\ & & & K_{dg} & K_{dd} \end{bmatrix} \begin{Bmatrix} x_u \\ x_f \\ x_r \\ x_g \\ x_d \end{Bmatrix} = \begin{Bmatrix} P_u \\ P_f \\ P_r \\ P_g \\ P_d \end{Bmatrix} \quad (2)$$

where subscript '*r*' denotes internal DOFs of the substructure S, subscripts '*f* ' and '*g*' represents the interface DOFs, '*u*' and '*d*' represents DOFs of the remaining structure. The equations of motion for substructure S may be extracted from the above system of global equations,

$$\begin{bmatrix} M_{rf} & M_{rr} & M_{rg} \end{bmatrix} \begin{Bmatrix} \ddot{u}_f \\ \ddot{u}_r \\ \ddot{u}_g \end{Bmatrix} + \begin{bmatrix} C_{rf} & C_{rr} & C_{rg} \end{bmatrix} \begin{Bmatrix} \dot{u}_f \\ \dot{u}_r \\ \dot{u}_g \end{Bmatrix}$$
$$+ \begin{bmatrix} K_{rf} & K_{rr} & K_{rg} \end{bmatrix} \begin{Bmatrix} u_f \\ u_r \\ u_g \end{Bmatrix} = \{P_r\} \quad (3)$$

The above equation can be rearranged to bring the 'interior' partitions to the left and interface effects in the form of a force on the right ,

$$M_{rr}\ddot{u}_r(t) + C_r\dot{u}_r(t) + K_r u_r(t)$$
$$= P_r - M_{rj}\ddot{u}_j(t) - C_{rj}\dot{u}_j(t) - K_{rj}u_j(t) \quad (4)$$

The subscript '*j*' denotes all interface DOFs (i.e. *f* and *g* included). In the above form it is required to calculate the substructure interface displacements, velocities and accelerations. These interface accelerations $\ddot{u}_j$ have to be obtained experimentally, and thereafter integrated to obtain the displacements and velocities. We also require the experimentally measured acceleration response $\ddot{u}_m$ at a few interior points *M*.

The estimated (or predicted) accelerations $\ddot{u}_e$ at those *M* points are obtained from the mathematical model from the left hand side of eq. (4). Here experiments are numerically simulated from responses generated from a known numerical model and may be artificially polluted with Gaussian noise of zero mean and 3% standard deviation for realism. Using an optimization algorithm such as GA or PSO we try to minimize the following fitness (objective) function, which is the sum of the square of deviations between the measured and estimated interior accelerations at all locations and all time

tions at all locations and all time steps,

$$f = \frac{\sum_{i=1}^{M}\sum_{n=1}^{L}\left|\ddot{u}_m(i,n) - \ddot{u}_e(i,n)\right|^2}{ML} \quad (5)$$

where subscript '*m*' and '*e*' denote measurement and estimated quantities respectively, *L* is the number of time steps and *M* is the number of measurement sensors used. Ideally it must be minimized to zero, but usually it approaches a small value close to zero.

3. Rrpresentation of a crack using orthotropic damage model

Based on continuum damage mechanics principle it is shown in [6] that a small material volume (SMV) with a line crack behaves as *effectively* orthotropic in a small zone. A small material volume with a crack can be represented as an equivalent continuum model with orthotropic properties producing the same strain at the boundaries of that volume. Thus the material behavior of the SMV with a line crack is expressed in terms of the *effectively* orthotropic elastic stiffnesses, which are the functions of the isotropic elastic stiffnesses, crack orientation and the size of the line crack. Thus, a change in the local elastic stiffness from initially isotropic to *effectively* orthotropic can be considered as the indicator of damage.

An elastic thin plate with thickness *h* and the width L_x and L_y in *x*- and *y*- directions, respectively (Figure 2) is considered in present study. The intact plate material is isotropic and posses Young's modulus *E* and Poisson's ratio *v*. Assume there is line crack of length 2*l* at (x_D , y_D) and aligned with the crack coordinate '1' which is oriented at θ with respect to the global coordinate *x*. The *effective* elastic stiffness Q_{ij}^D for the SMV containing a line crack damage is can be shown to be,

$$Q_{ij}^D = Q_{ij}(1 - e_{ij}D) \quad (i,j = 1,2,6) \quad (6)$$

where Q_{ij} are the reduced stiffness for the intact isotropic material in the plane stress state and e_{ij} are the *effective* material directivity parameters, given by

$$e_{11} = \frac{2\nu^2}{1-\nu^2},\ e_{22} = e_{12} = e_{21} = \frac{2}{1-\nu^2}$$
$$e_{16} = e_{26} = e_{61} = e_{62} = 0,\ e_{66} = \frac{2}{1+\nu} \quad (7)$$

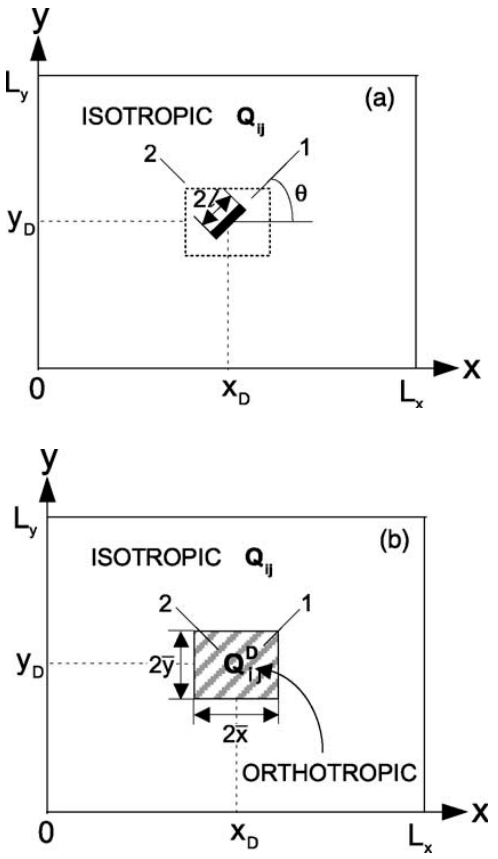

Figure 2. (a) Initially isotropic plate with a line through-crack and (b) its equivalent continuum damage representation in terms of effective orthotropic elastic stiffness

Thus *D* represents the averaged severity of damage within an SMV, which is called herein the *effective* damage magnitude. The

effective damage magnitude $0 \leq D \leq 1$ is defined by,

$$D = \frac{\pi h' l^2}{4\bar{x}\bar{y}h} \begin{cases} 0 \text{ for intact state} \\ 1 \text{ for complete material failure} \end{cases} \quad (8)$$

where h'= depth of the crack and h= thickness of plate; thus for a through crack $h'=h$. The effective orthotropic elastic stiffness Q_{ij}^{D} given by equation (6) are all measured with respect to the crack coordinates 1 and 2. Thus, the effective elastic stiffness with respect to the global coordinates x and y can be obtained by using the coordinate transformation as follows:

$$\bar{Q} = T(\theta)^T Q^D T(\theta) \quad (9)$$

where $T(\theta)$ is the coordinate transfer matrix, in which θ denotes the crack orientation (degrees) with respect to the global coordinate x. This approach has been implemented in a MATLAB based Finite Element model. Cracks of properties D and θ are assumed to be fully contained in one of the elements. It is also assumed that the crack does not propagate and the damping behavior remains unchanged. The proposed damage detection scheme has to identify location of the damaged element as well as the magnitude (*i.e.,* $D$and θ values) of the crack contained by it. The range of possible values are $0<D<1$ and $0<\theta<90^0$.

4. Genetic algorithm and particle swarm optimization

Genetic Algorithms are exploration algorithms based on the mechanism of natural selection and survival of the fittest. GA combines the explorative ability of large search spaces as well as reasonable guided search. GA creates an initial random sample within the specified domain of variables, called 'population'. It then ranks them in the order of fitness and conducts crossover operations from among a pool of 'parents' through the Roulette wheel selection. Parents having higher fitness have a greater probability of being selected and their offspring contribute to the next generation. GA can be programmed in the Binary or Continuous versions. Here, GA in the continuous (decimal number) version is used. It has been indicated in [13] and [14] that continuous GA is superior to binary GA in computational performance.

Particle swarm optimization (PSO) is a population based continuous optimization technique developed by Eberhart and Kennedy, inspired by the social behavior of bird flocking or fish schooling[15]. The system is initialized with a population of random solutions and searches for optima by updating generations. However, unlike GA, PSO has no evolution operators such as crossover and mutation. In PSO, the potential solutions, called particles, move through the problem space by following the current optimum particles. The basic PSO algorithm consists of the velocity and position equation:

$$\begin{aligned} v_i(k+1) = {} & \varphi(k)\, v_i(k) + \alpha_1[\gamma_{1i}(p_i - x_i(k))] \\ & + \alpha_2[\gamma_{2i}(G - x_i(k))] \end{aligned} \quad (10)$$

$$x_i(k+1) = x_i(k) + v_i(k+1) \quad (11)$$

i - particle index
k - discrete time index
v - velocity of i^{th} particle
x - position of the i^{th} particle/ present solution
p_i - historically best position/solution found by i^{th} particle
G - historically best position/solution found among all the particles.
$\gamma_{1,2}$ – random number in the interval (0,1) applied to i^{th} particle

An inertia term φ and acceleration constants $\alpha_{1,2}$ are also included. The inertia function is commonly taken as either as a constant or as a linearly decreasing function from 0.9 to 0.4.

The acceleration constants are usually set equal to 2. The values used in this paper for PSO parameters are referred from [16].

There are some indications from previous studies of the superiority of PSO over GA. For example the parameters of a Lorenz chaotic system were estimated using PSO [11]. It was found that PSO converges to the exact value with a high population size and was more computationally efficient than GA with the same population. Likewise a 10-dof structural dynamic model was identified using frequency response functions by GA and PSO - the latter was found to be superior to the former in accuracy and speed [17].

5. Condensation

Model condensation, whereby the number of DOF's in a model are reduced, is applied to the finite element model for faster computational performance. In this paper the rotational DOF's in the interior of the substructure are condensed out. There are two popular schemes *viz.,* (a) static or Guyan reduction scheme-GRS [18] and (b) the iterative improved reduction scheme-IRS [19] which is based on dynamic condensation requiring more computational effort. In GRS the rotational slave degrees of freedom are condensed out in the assumption that in the lower frequency modes their inertia forces are much less than those of the master DOFs. The errors in calculating the first 30 natural frequencies of the undamaged plate (used in the following numerical example) were calculated using both GRS and IRS and it was found that GRS errors were only about 3% for the 30^{th} natural frequency and were considered acceptable for the study. The range of the forcing frequency used here is also within the first few modes. The IRS errors were of course much smaller but at the expense of significant computational effort.

6. A numerical example

A simply supported thin aluminum plate with the following material properties is used as an example: thickness h= 0.004 m, dimension L_x= L_y = 0.5 m, Young's modulus E = 72Gpa, Poisson's ratio ν = 0.33 and mass density 2800 kg/m^3. The length of the line crack and its orientation are arbitrarily chosen. For example in one case the line crack is 0.032 m is located at the center of the plate, and orientation angle θ is 45^0. To compute the elastic stiffness Q_{ij}^D for a damaged zone (SMV), the dimension of the finite element is chosen as $2\bar{x} = 2\bar{y}$ = 0.04 m so that the effective damage magnitude for a crack length of 0.032 becomes D = 0.5. Table 1 shows the detailed comparison of natural frequencies of the intact and damaged plate at different damage orientations, while keeping D at 0.5. The natural frequencies have reduced in magnitude due to presence of crack damage and they are also dependent on damage orientation.

One fourth of the plate (top right corner) is taken as a substructure as shown in Figure 3. The full plate is divided in to 144 (12×12) finite elements and the substructure consists of 36 finite elements (6×6). Each node of the finite element has three DOFs, *viz.,* one transverse DOF and two rotational DOFs. The damage identification analysis is conducted to determine the damage magnitudes and orientations of all the finite elements.

A point harmonic force of 10sin (2π100t) N applied at the centre of the plate. The excitation frequency (100Hz) is above the first natural frequency of 77Hz. In the example considered here D = 0.5 and θ =45^0. The experiment is numerically simulated using a known mathematical model as mentioned in section 2. The synthetic responses of the numerical model are first calculated at all the interface and four interior points (see Figure3) in terms of displacement, velocity and acceleration using Newmark's method with constant time step of 0.001 sec for 2 seconds using the harmonic force.

Section 6.1 discusses the case where the effect of noise in acceleration measurements is ignored, and Section 6.2 takes into account signals with Gaussian noise of zero mean and 3% standard deviation, and another forcing frequency of 200Hz.

Table 1. Natural Frequencies of Simply Supported plate with different crack orientations θ (Damage magnitude (D)= 0.5)

Mode No.	Intact	$\theta = 0^0$	$\theta = 15^0$	$\theta = 30^0$	$\theta = 45^0$
1	77.529	75.441	75.302	75.019	74.876
2	193.24	192.09	191.83	191.24	190.83
3	193.24	192.94	192.98	193.02	193.01
5	386.35	370.77	368.62	364.8	362.95
10	657.49	652.57	653.81	654.98	654.97
20	1163.5	1162.6	1160.3	1154.1	1149.5
30	1661.8	1653.5	1654.1	1652.9	1650.6

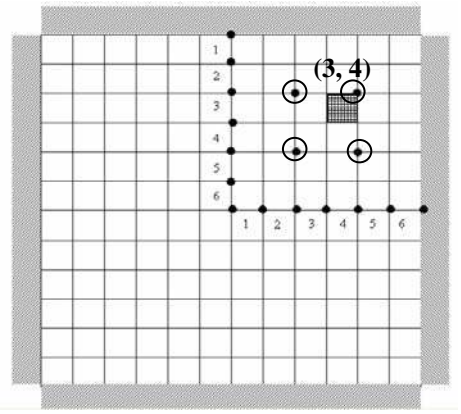

Figure 3. Aluminium plate with damaged element (3,4) inside the substructure
⦿ Acceleration measurement points at substructure interface and interior

6.1. Global and substructure approaches

Four situations are studied here *viz.,* identification with:

a) uncondensed substructure matrix
b) condensed substructure matrix
c) uncondensed global matrix
d) condensed global matrix.

The performance of GA and PSO is also compared here.

Table 2 shows the summary of DOF's in the substructure. The substructure consists of 36 elements with 147 DOFs. PSO parameters are set as 1000 particles (swarm size), maximum 50 generations (iterations), a linearly decreasing inertia function from 0.9 to 0.4, and acceleration constant set to 2. GA is also set to 1000 particles with crossover rate of 40% and mutation rate of 1%. These algorithms have to identify a total of 72 unknowns, viz., 36 damage magnitudes and 36 damage orientations for each finite element.

First we consider the case of the uncondensed quarter substructure. The damage identification results are shown in Figure 4 in a three-dimensional chart form, at various stages of iteration (1st, 25th and finally

the 30th iteration after convergence occurs). The data for D are shown on the left hand and θ on the right hand side. PSO has identified the location of the damage i.e., element (3, 4) with damage magnitude, D = 0.53 and damage orientation, $\theta = 44.2^0$ at the 30th generation. The accuracy is good considering the exact values of D = 0.5 and $\theta = 45^0$.

To show the fast convergence of PSO algorithm compared with GA, the same problem has been solved by minimizing the fitness function by GA, as shown in Figure 5. The identification of damage by GA at the 30th iteration, is far from converged to the final values, compared to the situation with PSO of the same population size and number of generations.

Table 2. Summary of DOFS of the substructure

	Full Structure	Substructure	
		With out condensation	With condensation
Total DOFs	507	147	75
No. of interface DOFs	---	39	39
No. of internal DOFs	---	108	36
No. of unknowns	144	36*2	36*2

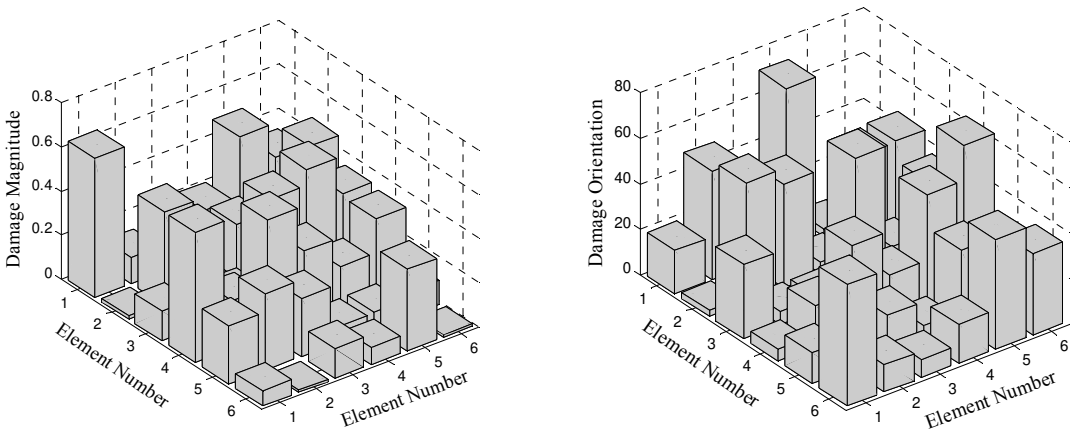

Figure 4. (a): Damage identification-PSO 1st Generation

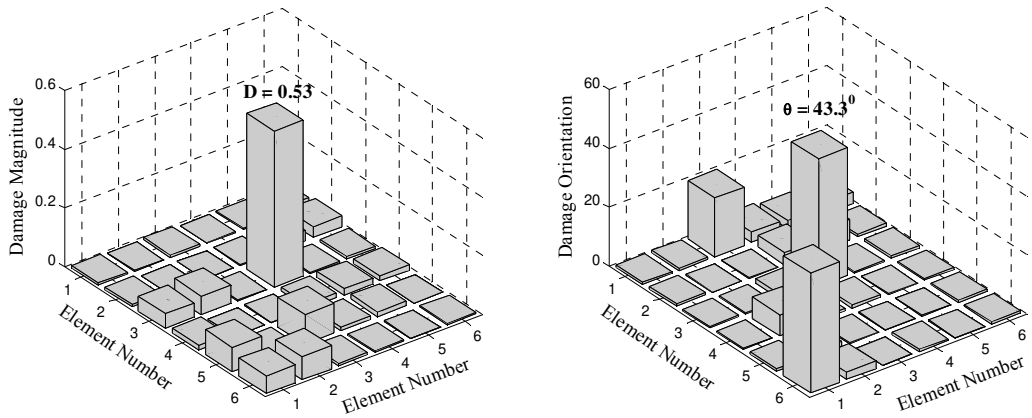

Figure 4. (b): Damage identification - PSO 25th Generation

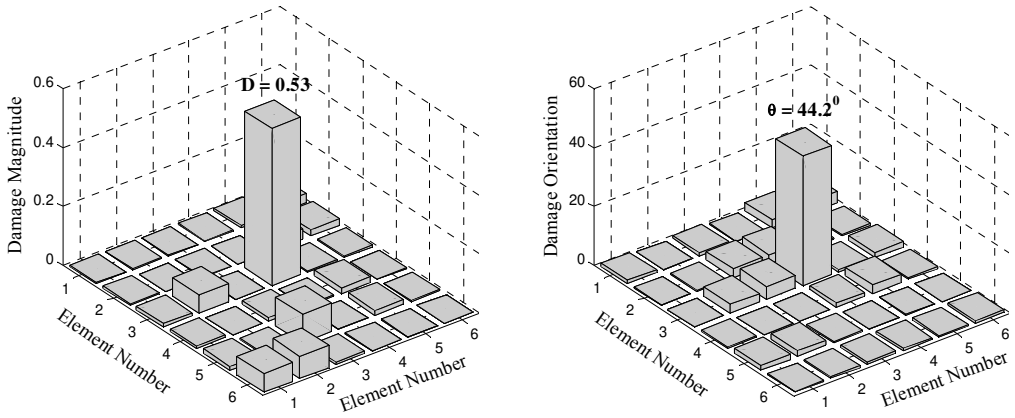

Figure 4. (c): Damage identification-PSO 30th (final) Generation

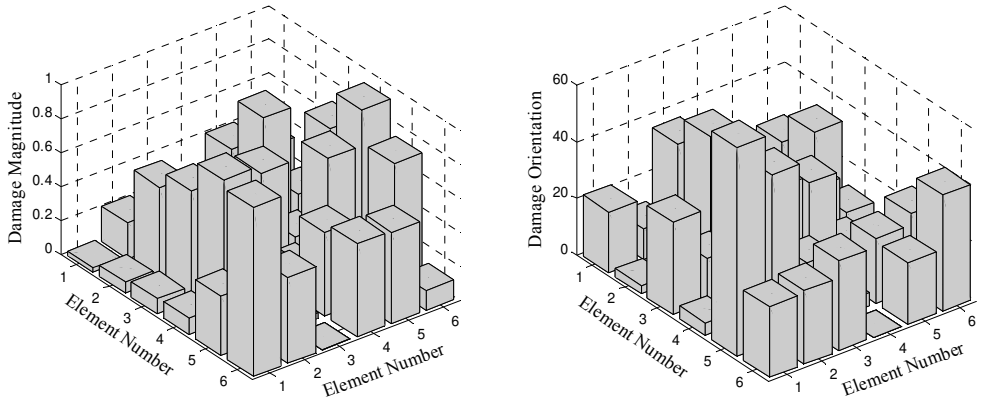

Figure 5. Damage identification-GA at 30th generation

Next, Figure 6 shows a typical example of convergence fitness function of PSO compared with GA with respect to generations. The trend in decrease of the fitness value appears to be the same for both algorithms until the 5th generation. Thereafter GA has been stuck in a local optima where as PSO is converging at a fast rate towards the global minima. GA continues to converge very slowly; it needs more generations to reach the global minima of zero. Thus, PSO has proved to have a good convergence and accuracy compared to GA. Hence in the examples hereafter only PSO is used to identify damage.

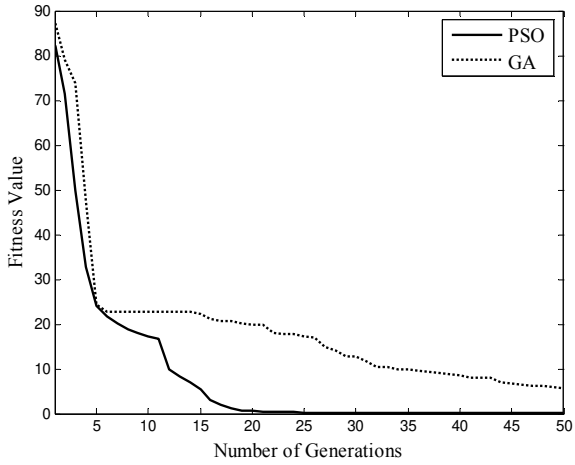

Figure 6. Comparison of convergence of PSO and GA

Next we compare the convergence and accuracy of identification when using the condensed substructure matrix. The same PSO parameters as in the previous case are used here. The saving in computational time when using this approach is shown in Table 3. The total time taken to identify the condensed structure is 1333 seconds, which includes 218 seconds taken up by the Guyan reduction and the remainder by various other operations. This may be favourably compared to 2248 seconds (total) for the uncondensed substructure, which results in about 40% savings of computational effort.

Using the condensed matrix, Figure 7 (a) and (b) shows that PSO has identified exactly the location of the damage i.e., element (3,4) with damage magnitude $D = 0.48$ and damage orientation $\theta = 46^0$, whereas actual damage variables are $D = 0.5$ and $\theta = 45^0$. However it has taken almost 50 generations to obtain the same accuracy which was obtained in 35 generations in the previous case of uncondensed substructure. This could be attributed to the Guyan approximation in condensation. The following Figure 8(a) and (b) show the convergence of identification of damage index D and orientation angle θ for the damaged element (3,4) and a neighboring undamaged element (2,3) for comparison. The slower convergence of the orientation angle θ as compared to damage index D is also seen here. Both indices finally converge to zero for the undamaged element.

Next the method of Global structure damage identification is attempted. The same PSO parameters are used as in above examples. The total numbers of unknown damage parameters in the uncondensed Global matrix is quite large: namely 144 damage magnitudes and 144 damage orientations (total of 288) for all the 144 elements (Ref Table.4). Thus there are 288 optimization variables in the PSO algorithm which would definitely appear beyond its numerical capabilities. Table 4 also gives the time taken for 50 iterations under these circumstances, which are 18 hours for the uncondensed matrix and 7.32 hours for the condensed matrix.

Figure 9 shows the poor convergence of fitness function when using the Global model (condensed and uncondensed). The fitness function is not minimized to anywhere close to zero in the specified 50 iterations. Understandably in this case, the estimated values for D and θ (shown for element (3, 4) in Table 5) is very poor in accuracy. This example shows the efficiency of substructure methods.

Table 3. Reduction in CPU time with condensing internal DOFs of the substructure

Method	Total time (sec)	GRS (sec)	Total saving in time (%)
Uncondensed	2248	--	--

Condensed	1333	218	40.7

Table 4. Summary of DOFS of the Full Structure

	Full Structure	
	With out condensation	With Condensation
Total DOFs	507	169
No. of unknowns	144*2	144*2
Computational time (hrs)	18.16	7.32

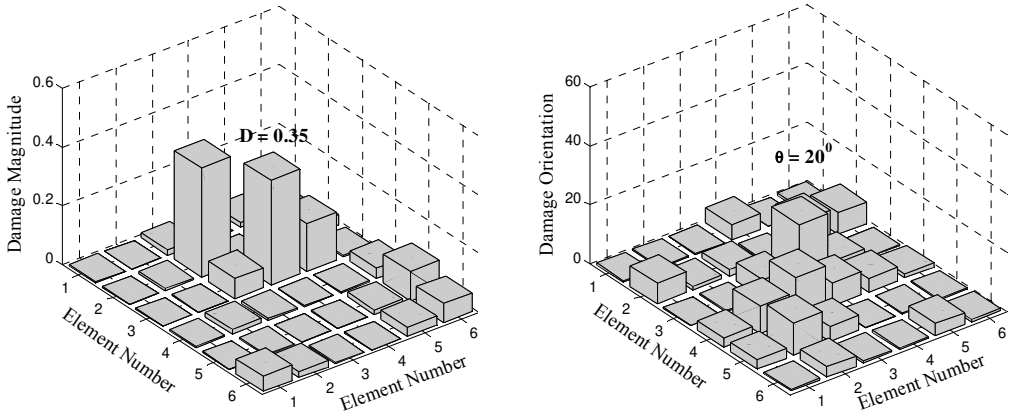

(a) After 35th generation

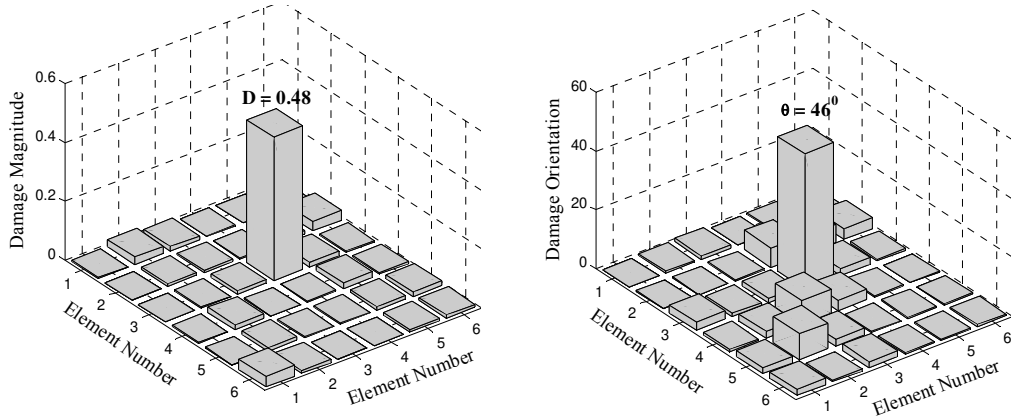

(b) Identified after 50 generations

Figure 7. Damage identification for condensed substructure using PSO

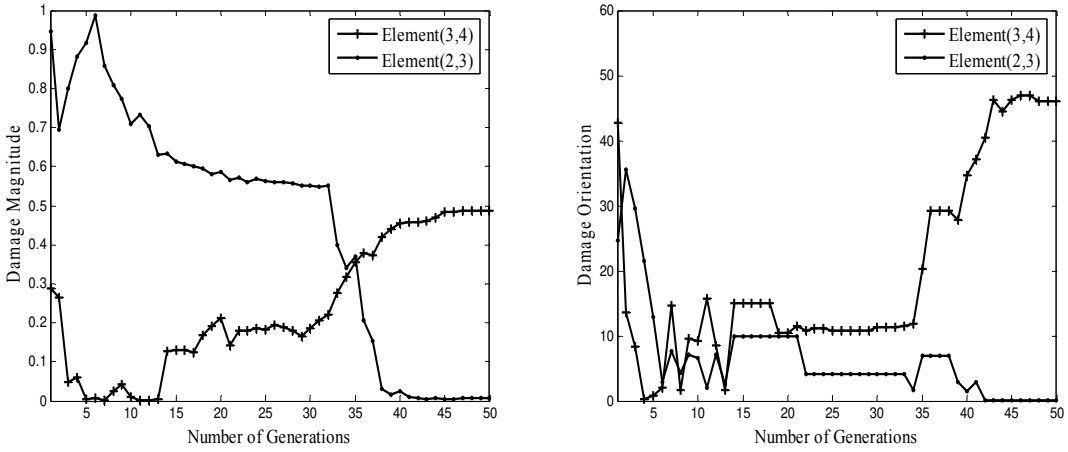

Figure 8. Convergence of (a) damage magnitude (b) orientation of elements

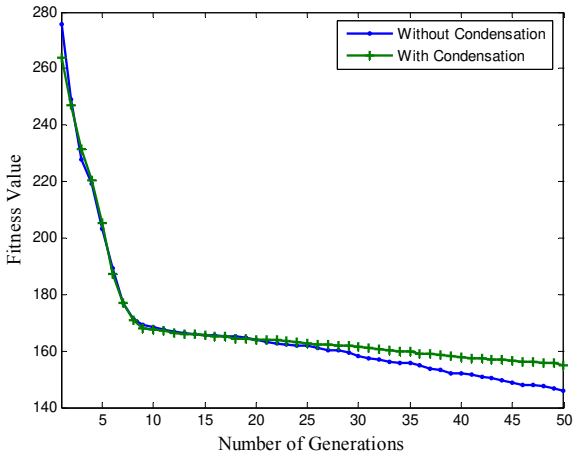

Figure 9. Objective function convergence: Global uncondensed and condensed cases.

6.2. Effect of noise and different forcing frequency

This section very briefly looks at two cases (a) the acceleration measurements are polluted by Gaussian noise of zero mean and 3% standard deviation and (b) additionally the harmonic excitation is changed to a new frequency of 200 Hz. The cases are studied using the condensed substructure approach. The plate properties and damage case are the same as in section 6.1 *i.e.,* the crack damage variables are $D = 0.5$ and $\theta = 45^0$ and occur in element (3, 4). Figure 10 shows the 3-D damage identification chart using PSO at the 50^{th} generation for case (a). It is seen that due to presence of noise, D and θ are predicted as 0.46 and 43.5^0 respectively (i.e., with 8% and 5.5% error). Also quite a few other undamaged elements have not converged to zero values of D and θ. Figure 11 shows the slow convergence of the fitness function for this noisy case compared to the zero-noise case studied in section 6.1.

Next Figure 12 shows the same type of 3-D damage identification plot for case (b) *i.e.,* at 200Hz excitation. Due to presence of noise, here D and θ are predicted as 0.55 and 48.6^0 respectively (i.e., with 10% and 8% error). Here also quite a few other undamaged elements have not converged to zero values of D and θ. Figure 13 shows the convergence of the fitness function at 200Hz excitation and it follows the same trend as Figure 11.

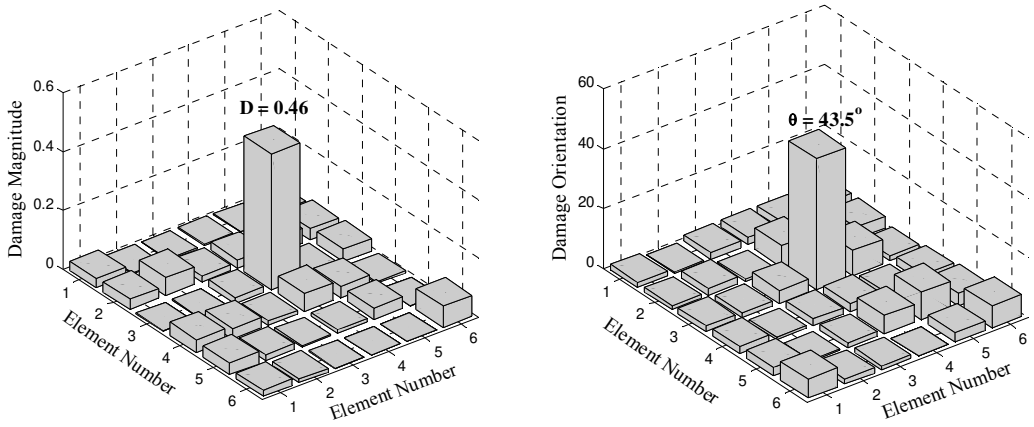

Figure 10. Damage identification with 3% noise and 100Hz excitation – PSO at 50th Generation.

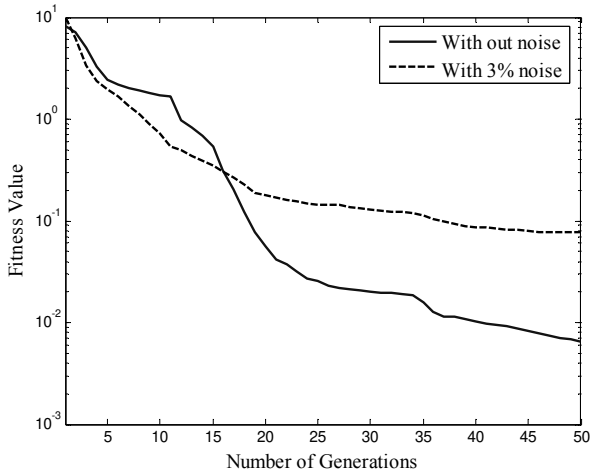

Figure 11. Convergence of fitness function (100 Hz excitation) with 3% noise

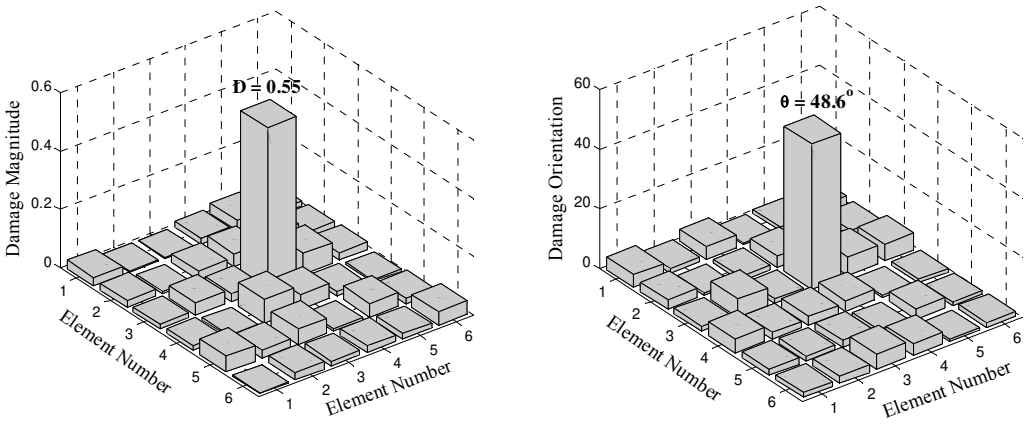

Figure 12. Damage identification with 3% noise and 200Hz excitation – PSO at 50th Generation.

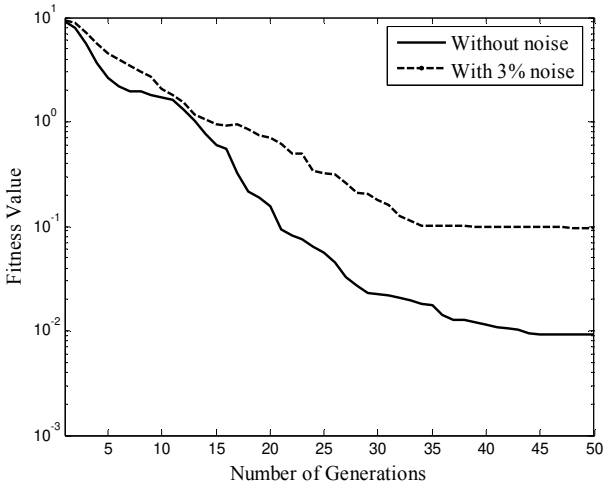

Figure 13. Convergence of fitness function (200 Hz excitation) with 3% noise

7. Conclusions

A time domain response based damage identification scheme is applied to a thin uniform plate with a crack contained in a finite element. The isotropic element containing the crack is considered as an equivalent element with orthotropic properties producing the same strain at the boundary. The method was able to correctly predict the location as well as damage magnitude and angle of a crack using numerically simulated experiments on a finite element model. Damage identification using a global model of the plate was found to be prohibitively computationally expensive. A quarter substructure was identified and significant improvements in computational effort were noted. A 40% further saving in time was noted when the substructure was further condensed of the rotary DOF's, The crack parameters were correctly identified when there was zero noise in the acceleration measurements, and with about 8-10% error when 3% noise was introduced. The method also works well for different forcing frequencies.The Particle Swarm algorithm was found to be superior in convergence and accuracy compared to the conventionally used Genetic Algorithm.

References

[1] Doebling, S. W., Farrar, C. R., Prime, M. B., and Shevitz, D. W. 1996. "*Damage identifcation and health monotoring of structural and meachincal systems from changes in their vibration characteristics: a Literature review*" LA-13070-MS. Los Alamos National Laboratory.

[2] Lee, Y. S., and Chung, M. J. 2000. A study on crack detection using eigenfrequency test data. *Computers and Structures*, 77: 327-342.

[3] Wang, X., Hu, N., Hissao, Fukunaga., and Yao, Z. H. 2001. Structural damage identification using static test data and changes in frequencies. *Engineering Structures*, 23: 610-621

[4] Hwang, H. Y., and Kim, C. 2004. Damage detection in structures using few frequency response measurements. *Journal of Sound and Vibration*, 270: 1-14.

[5] Araujo dos Santos, J. V., Mota Soares C. M, Soares, C. A., and Maia, N. M. M. 2005. Structural dmage identification in laminated structures using FRF data. *Composite Structures*, 67: 239-249.

[6] Lee, U., George A Lesieutre., and Lei, Fang. 1997. Anisotropic damage mechanics based on strain energy equivalence and equivalent elliptical microcracks. *International Journal of Solids and Structures*, 34: 4377-4397.

[7] Lee, U., Cho, K., and Jinho, Shin. 2002. Identification of orthotropic damages within a thin uniform plate. *International Journal of Solids and Structures*, 40: 2193-2213.

[8] Huiwen, H., Wang, B. T. Lee, C. H., and Su, J. S. 2006. Damage detection of surface cracks in composite laminates using modal analysis and strain energy method. *Composite Structures*, 74: 399-405.

[9] Koh, C. G., Hong, B., and Liaw, C. Y. 2003. Substructural and progressive structural identification methods. *Engineering Structures*, 25: 1551-1563.

[10] Hong, H., and Young X. 2002. Vibration based damage detection of structures by genetic algorithm *Journal of Computing in Civil Engineering*, 16(3): 22-229.

[11] He, Q., Wang, L., and Liu, B. 2007. Parameter Estimation for Chaotic Systems by Particle Swarm Optimization. *Chaos, Solitons and Fractals*, 34: 654-661.

[12] Clough, R. W., and Penzien, J. 2003, "*Dynamics of Structures*", Mc Graw Hill International Edition, 2003.

[13] Michalwicz, Z. 1994. "*Genetic Algorithms + Data structures = Evolutionary Programs*" AI Series, Springer Verlag, New York.

[14] Haupt, R. L. 1999. "*Practical Genetic Algorithms*" John Wiley and Sons, New York.

[15] Eberhant, R. C., and Kennedy, J. 1995. A New Optimizer using Particle Swarm Theory. *Proceedings Of the 6th International Symposium on Micro Machine and Human Science,* Nagaya, Japan

[16] Shi, Y., and Eberhart, R. 1998. Parameter selection in particle swarm optimization. *Proceeding of the 7th Annual Conference on Evolutionary Programming*, *EP98.* San Diego, U. S. A.

[17] Mouser, C. R., and Dunn, S. A. 2005. Comparing Genetic Algorithm and Particle Swarm Optimization for Inverse Problem. *ANZIAM Journal*, 46(e): 89-101.

[18] Guyan, R. J. 1965. Reduction of stiffnesses and mass matrices. *AIAA Journal*, 3(2): 380-385.

[19] Friswell, M. I., Garvey, S. D., and Penny. 1995. Model reduction using dynamic and iterated IRS techniques. *Journal of Sound and Vibration,* 186: 311-323.